Structure, Vol. 11, 411–422, April, 2003, ©2003 Elsevier Science Ltd. All rights reserved. DOI 10.1016/S0969-2126(03)00047-9

Symmetry Recognizing Asymmetry: Analysis of the Interactions between the C-Type Lectin-like Immunoreceptor NKG2D and MHC Class I-like Ligands

Benjamin J. McFarland,[1] Tanja Kortemme,[2] Shuyuarn F. Yu,[1] David Baker,[2] and Roland K. Strong[1,*]
[1]The Division of Basic Sciences
Fred Hutchinson Cancer Research Center
1100 Fairview Avenue North
Seattle, Washington 98109
[2]Howard Hughes Medical Institute and
Department of Biochemistry
University of Washington
J Wing
Health Sciences Building
Seattle, Washington 98195

Summary

Engagement of diverse protein ligands (MIC-A/B, ULBP, Rae-1, or H60) by NKG2D immunoreceptors mediates elimination of tumorigenic or virally infected cells by natural killer and T cells. Three previous NKG2D-ligand complex structures show the homodimeric receptor interacting with the monomeric ligands in similar 2:1 complexes, with an equivalent surface on each NKG2D monomer binding intimately to a total of six distinct ligand surfaces. Here, the crystal structure of free human NKG2D and in silico and in vitro alanine-scanning mutagenesis analyses of the complex interfaces indicate that NKG2D recognition degeneracy is not explained by a classical induced-fit mechanism. Rather, the divergent ligands appear to utilize different strategies to interact with structurally conserved elements of the consensus NKG2D binding site.

Introduction

Natural killer (NK) cells mediate early immune system responses against cells undergoing neoplastic transformation or infection by viruses or intracellular parasites [1]. They function through a diverse array of cell surface receptors that can be divided into two families by structural homology: NK receptors (NCRs) with immunoglobulin-like ectodomains (such as KIRs, LIRs, and NKp46), or C-type lectin-like ectodomains (NKDs; including the NKG2x/CD94 family, the Ly49x family, and NKR-P1) [2, 3]. NK cell activation occurs through integration of the activating and inhibitory signals across the constellation of NCRs engaged upon interrogation of target cells [4, 5].

Many NCRs recognize classical (HLA-A, -B, and -C) and nonclassical (HLA-E) major histocompatibility complex (MHC) class I proteins and occur in paired activating and inhibitory isoforms. MHC molecules bind peptides derived from endogenous proteins and then traffic to the cell surface, providing a means for T cells to monitor the proteome of a given cell for pathogen- or tumor-associated protein expression. However, many viruses and tumors evade T cell surveillance by simply downregulating MHC class I expression [6]. NK cells in the periphery stochastically express a subset of activating and inhibitory MHC class I-specific NCRs, selected so that normal MHC expression prevents NK cell activation, whereas loss of any MHC class I allele tilts the NCR signal toward activation, providing a back-up for T cell surveillance [5]. However, some viruses encode decoy ligands for inhibitory NCRs that circumvent this system [7].

NKG2D is a homodimeric, activating NKD-type NCR distantly related to other members of the NKG2 family (20%–30% identical), which otherwise normally assemble as heterodimers with CD94 [8–10]. NKG2D was originally identified on NK cells but has subsequently been found broadly expressed on macrophages, $\gamma\delta$, and $CD8^+$ $\alpha\beta$ T cells. Rather than binding true MHC class I proteins, NKG2D ligands include the MIC (-A and -B, which are ~84% identical overall) and ULBP (1, 2, and 3; 55%–60% identical pairwise) proteins in primates or H60 and the retinoic acid-inducible Rae-1 family of proteins (α, β, γ, and δ; ≥92% identical pairwise) in rodents. Whereas murine (muNKG2D) and human NKG2D (huNKG2D) are 69% identical in their ectodomains, their ligands are quite dissimilar in sequence, with overall pairwise sequence identities from 23% to 27%.

All currently characterized NKG2D ligands are distant structural homologs of MHC class I proteins [11–13]. However, unlike true MHC class I proteins, the NKG2D ligands bind neither antigenic peptides (or any other small molecule ligand) nor β_2-microglobulin, and ULBP3 and Rae-1β even dispense with the α3 domain, existing as isolated $\alpha1\alpha2$ platform domains membrane anchored by GPI linkages. NKG2D-ligand interactions are also tighter (K_ds in the 1 to 0.01 μM range) than other NCR- or TCR-ligand complexes (K_ds in the 10 to 100 μM range) [10, 12]. Also unlike MHC class I proteins, which are constitutively expressed on almost all cell types, many NKG2D ligands are expressed conditionally and only by certain cells [10]. For example, MIC-A expression is induced by cellular stress on gastrointestinal epithelium and epithelially derived tumors. NKG2D engagement of MIC ligands dominantly activates effector responses from NK cells and $\gamma\delta$ T cells, and may costimulate $CD8^+$ $\alpha\beta$ T cell responses. In mice, Rae-1 or H60 expression drives NK-mediated tumor rejection. NKG2D-ligand interactions therefore mediate crucial antiviral and antitumor innate immune responses in response to low-level signals like cellular stress.

Crystal structures are now available for muNKG2D [14] and huNKG2D (reported here); MIC-A [11], MIC-B [15], and Rae-1β [13]; and for the complexes between huNKG2D and MIC-A [16], huNKG2D and ULBP3 [12], and muNKG2D and Rae-1β [13]. The symmetric NKG2D homodimers bind their asymmetric, monomeric ligands in a 2:1 molar stoichiometry. Equivalent binding sites on

Key words: immunoreceptors; MHC class I homologs; structural immunology; molecular recognition; computational alanine scanning; interface plasticity

*Correspondence: rstrong@fhcrc.org

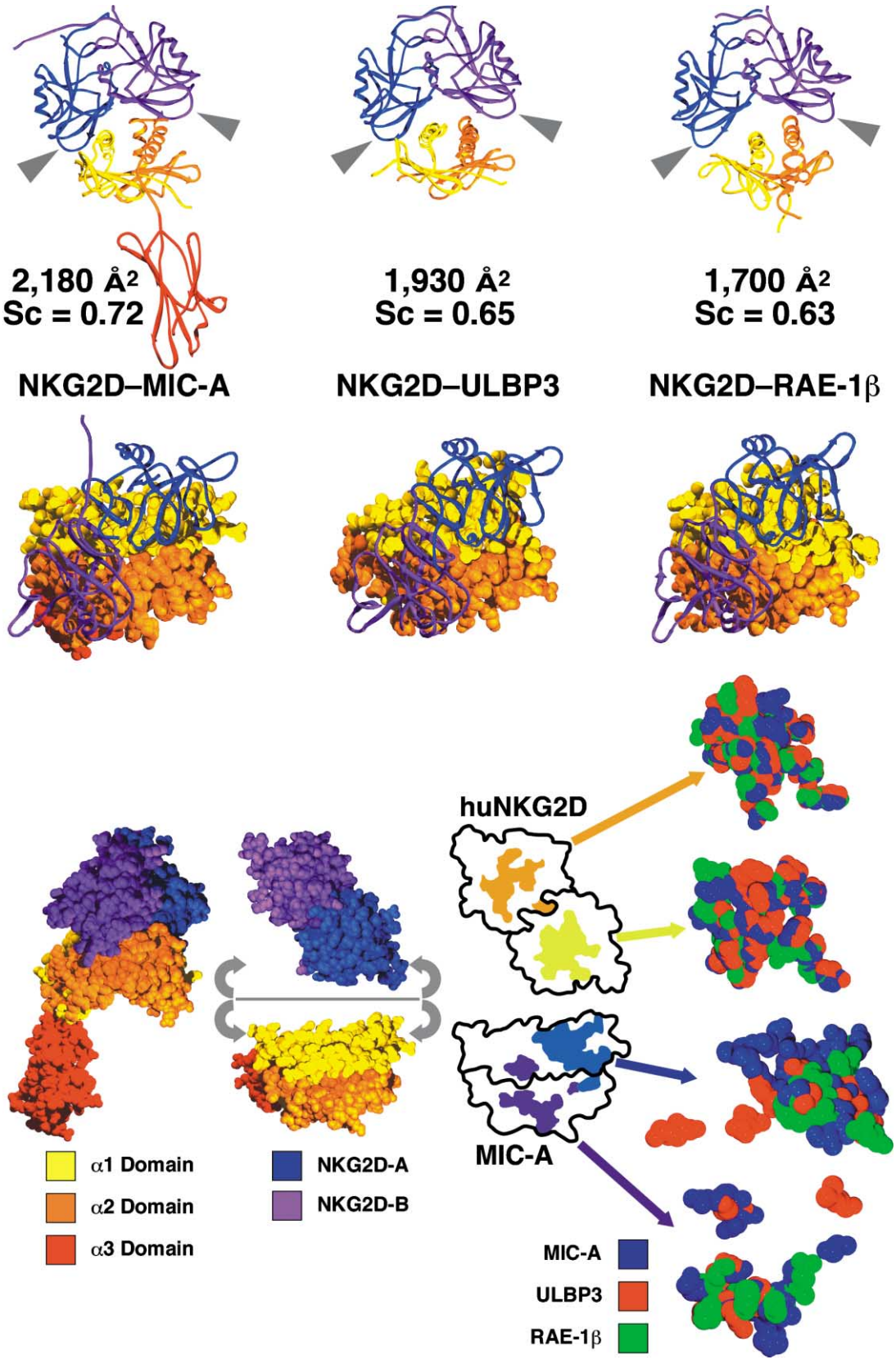

Figure 1. Structures of NKG2D-Ligand Complexes

Top: views of three NKG2D-ligand complex structures are shown, with each complex shown in paired views; one view of the side of the complex (above), with the protein backbones shown in a ribbon representation; the other view (below), looking down onto the top of the

each NKG2D monomer contribute nearly equally to an extensive interface where each receptor monomer binds a distinct ligand surface (Figure 1). All three NKG2D complexes are quite similar overall, despite the dissimilarity in detail between the structures of the ligand proteins: ligand pairwise root-mean-square deviations (rmsd) range from 3.8 to 5.8 Å (calculated on fairly restricted Cα sets due to the high degree of mismatch). The saddle-shaped NKG2D homodimer sits astride the platform domain of the MHC class I-like ligands, with each NKG2D monomer primarily contacting either the α1 or α2 subdomain of each ligand. Each NKG2D monomer-ligand subdomain (α1 or α2) pair constitutes a "half-site" in our terminology. The footprints of the ligands on each of the six NKG2D half-sites essentially overlap (Figure 2), showing that NKG2D truly utilizes a single binding site consisting of residues from the body of the NKG2D NKD and one loop (β5′-β5). This loop, referred to as the "stirrup" loop [16], is the most distal element of NKG2D that contacts ligand. The single NKG2D binding site has therefore evolved to recognize at least six different surfaces, predominantly on the α1 or α2 domains of MIC-A, ULBP3, and Rae-1β, with dramatically different shapes (Figure 1). Additionally, many of the very nonconservative sequence differences and deletions between MIC-A and MIC-B alleles and ULBP3 and Rae-1 isoforms map to NKG2D-contacting residues (Figure 3) [12, 13, 15].

Two conceptually different solutions to this binding problem can be envisioned: first, extensive plasticity allows the receptor to rearrange its binding site according to the requirements of the ligand (induced-fit). Second, divergent ligands may utilize different strategies to recognize an essentially identical receptor binding site. In order to investigate the recognition mechanism that allows for such extreme ligand degeneracy while maintaining relatively high affinities and selectivities, we report here the results of (1) the crystallographic analysis of huNKG2D crystallized alone at 2.5 Å resolution to complete the examination of potentially flexible interface elements and (2) in silico and in vitro alanine-scanning mutagenesis analyses of the three available complex structures to quantitate the relative contributions different residues make to the binding interactions. The results show that binding energy is unevenly distributed across the interfaces, with "hotspots" associated with structurally conserved receptor elements, thus arguing against an induced-fit recognition mechanism.

Results

The NKG2D-ligand interfaces are extensive, highly shape complementary, and involve a mixture of interaction types not dominated by hydrophobic terms: only 55%–62% of the solvent-accessible surface area buried in the complexes is nonpolar (Figures 1, 2, and 3). In contrast, many other protein-protein interactions are largely mediated through highly adaptive hydrophobic surfaces [17]. For NKG2D, electrostatic interactions contribute but do not dominate (with the exception of the muNKG2D-H60 complex) [12, 18] as they do for the KIR complexes [19, 20]. Moreover, the residue pairs forming salt bridges in the complexes are variable (Figures 2 and 3). Beyond the salt bridges and similarly variable hydrogen bonds and van der Waals interactions (Figures 2 and 3), three common residue positions at the center of each half-site do make direct contacts with ligand in all six half-sites (binding site "core" residues): Tyr152, Met184, and Tyr199 (Tyr168, Ile200, and Tyr215 in muNKG2D). Both tyrosine side chains point toward the ligand in all six half-site structures, with their centers separated by about 6 or 7 Å, depending upon Tyr152 rotamer utilization (see below). In addition to other contacts, the tyrosine side chains generally sandwich the side chain of another residue, but the range of residue types, and the nature of the contacts in the sandwich, is quite diverse: a methionine in the α1 MIC-A and ULBP3 α2 half-sites (the latter methionine displacing the partially sandwiched Met184 from huNKG2D as in the other three huNKG2D complex half-sites), a leucine in the ULBP3 α1 half-site, and either an arginine, making cation-π contacts to both tyrosines, or a phenylalanine, making both en face and herringbone contacts, in the two muNKG2D half-sites.

It has been proposed [12, 21] that NKG2D binding degeneracy can be explained through a classical induced-fit mechanism, a term first coined to describe the molding of a flexible, malleable enzyme binding site into the complement of its cognate substrate concurrent with binding [22]. The immune system utilizes classical induced-fit receptor-ligand interactions in the interactions between antibodies and antigens, such as the ligand-induced changes in the antigen binding fragment of the anti-influenza virus hemagglutinin peptide antibody 17/9 [23], and between αβ TCRs and MHC class I proteins [24–27]. Both examples involve dramatic movements of the backbone atoms of key receptor ligand binding loops of 3 to 6 Å and side chain movements of up to 15 Å at the distal atom.

Elements of Flexibility in NKG2D

The most flexible part of the receptor is the 21 residue long N-terminal stalk of the ectodomain (huNKG2D; residues 75–95) between the NKD and the membrane-span-

ligand from the perspective of the receptor-bearing cell, with the receptor represented as a backbone ribbon and the ligand as a CPK model. Secondary structure elements are portrayed as β strands, arrows; α helices, coils in the ribbon representations. Proteins are colored by domain: MHC class I-like ligands are colored as α1, yellow; α2, orange; and α3 (when present), red; the receptor domain over the ligand α1 domain is colored blue and the domain over the α2 domain is colored purple. Arrows indicate the stirrup loops of NKG2D in the various complexes. Buried solvent-accessible surface areas (Å^2) and shape complementarity (Sc) values are also shown. Figures were generated with SwissPDB-Viewer [47] and rendered with POV-RAY3 (http://mac.povray.org).

Bottom: in order to generate schematic representations of the binding interfaces, complexes are split open, with the domains oriented looking down onto the contact surfaces. The proteins are then outlined and the contact surface is displayed as a colored patch. On the right, CPK representations of superpositions (based on the NKG2D monomer from each half-site) of the contact residues from all of the three complex structures are shown, with NKG2D surfaces in the upper frames and ligand surfaces shown in the lower frames as indicated. This demonstrates the relative structural conservation of atoms in the receptor binding sites and the structural diversity of atoms comprising the receptor-contacting residues in the ligands.

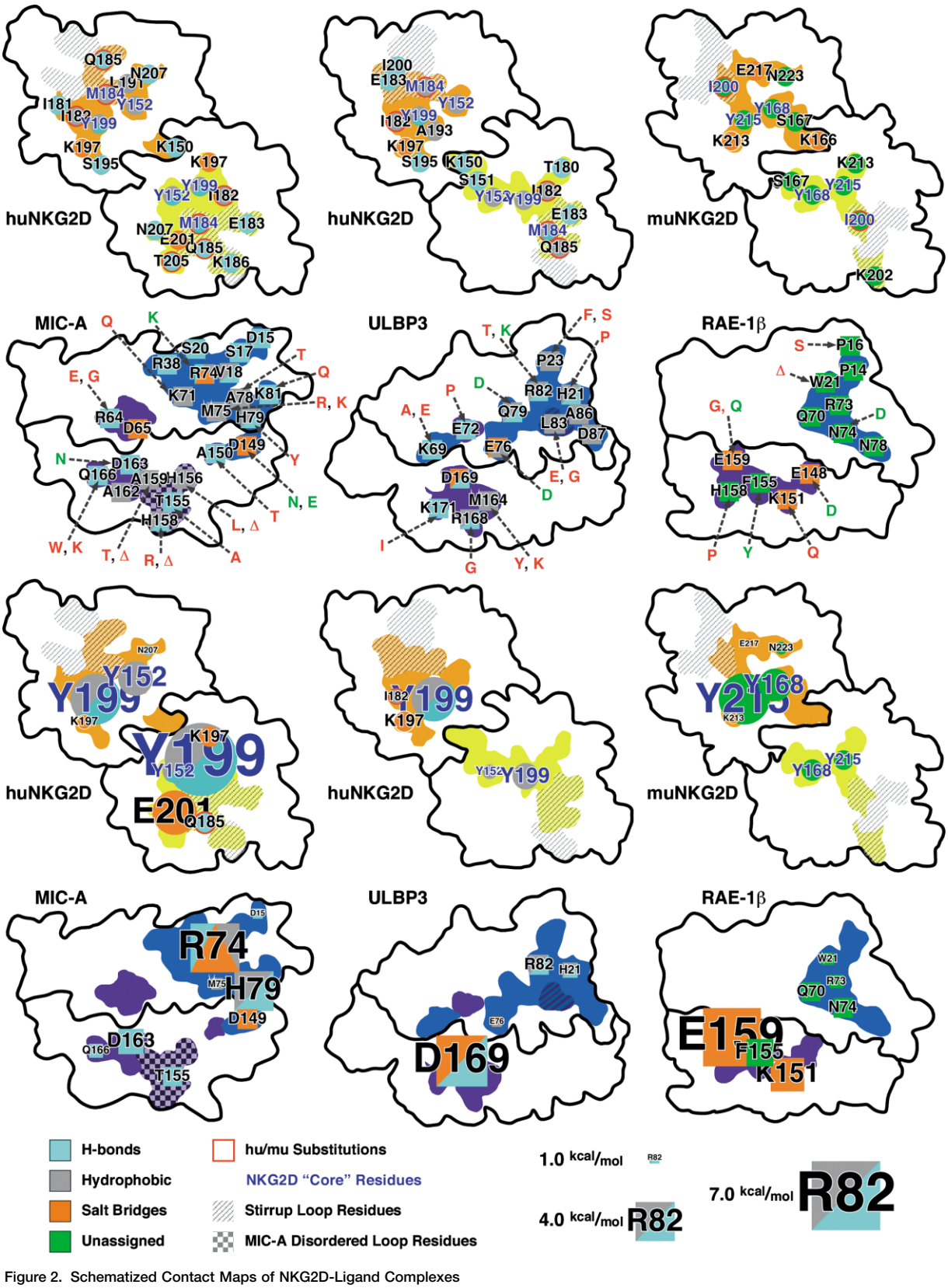

Figure 2. Schematized Contact Maps of NKG2D-Ligand Complexes

Top: contact residues have been mapped onto schematized representations of the three complex structure interfaces. Binding surfaces are displayed as colored patches. Each residue is labeled, and its corresponding tag (squares for ligand residues, circles for receptor residues) is colored by the type of interaction it makes with its cognate contact on the opposite surface, as indicated. Receptors are shown across the top and ligands across the bottom of the frame. Ligand-contacting residues in the stirrup loops of the receptors are represented by crosshatched

Human NKG2D	MICA Contact	ULBP3 Contact	Murine NKG2D	RAE-1 Contact
A-chain				
Lys150	*No contact*	Glu76, Glu76	Lys166	*No contact*
Ser151	*No contact*	Gln79	Ser167	Gln70
Tyr152	Lys71, Arg74, Met75,	Gln79, Arg82, Leu83	Tyr168	Arg73, Trp21, Gln70
Thr180	*No contact*	Lys69	Thr196	*No contact*
Ile182	His79	Ala86, Asp87	Val198	*No contact*
Glu183	Lys81	His21	Glu199	*No contact*
Met184	Val18, Val18, Arg74, Ala78	His21, His21, Arg82, Ala86	Ile200	Pro14
Gln185	Val18	Pro23	Pro201	*No contact*
Lys186	Asp15, Ser17	*No contact*	Lys202	Pro16
Lys197	Asp149	*No contact*	Lys213	Asn78
Tyr199	Met75, His79	Leu83	Tyr215	Asn74, Arg73
Glu201	Arg74	*No contact*	Glu217	*No contact*
Thr205	Ser20	*No contact*	Asn221	*No contact*
Asn207	Arg38	*No contact*	Asn223	*No contact*
B-chain				
Lys150	Ala150	*No contact*	Lys166	Glu148
Ser151	*No contact*	*No contact*	Ser167	Glu148
Tyr152	His156, Ala159	Met164	Tyr168	Lys151, Phe155
Ile181	Gln166	*No contact*	Leu197	*No contact*
Ile182	Ala162, Gln166	Arg168	Val198	*No contact*
Glu183		Lys171	Glu199	*No contact*
Met184	His158, Ala162	Arg168, Lys171	Ile200	His158
Gln185	His158	*No contact*	Pro201	*No contact*
Leu191	Thr155	*No contact*	Val207	*No contact*
Ala193	*No contact*	Leu83	Gly209	*No contact*
Ser195	Arg64	Glu72	Ser211	*No contact*
Lys197	Asp65	Asp169	Lys213	Glu159
Tyr199	Asp163, Ala159	Met164, Arg168, Asp169	Tyr215	Glu159, Phe155
Ile200	*No contact*	Arg168	Thr216	*No contact*
Glu201	*No contact*	*No contact*	Glu217	Lys151
Asn207	Thr155	*No contact*	Asn223	Lys151

Figure 3. Tabulation of NKG2D-Ligand Contacts

Residue-residue contacts have been tabulated from the original structure references [12, 13, 16], with ligand residues colored by the type of interaction observed as in Figure 2. Receptor murine/human sequence differences are colored red.

ning domain (NKG2D is a type II transmembrane protein). Although the various crystallization constructs encompass most, if not all, of this region, at most only about a quarter, and typically only a few residues, of the stalk is ordered. However, while extremely flexible, the stalks cannot contribute to induced-fit recognition because they are distal to the ligand binding sites.

A large degree of flexibility is also displayed by NKG2D at the homodimer interface. Structures of free muNKG2D [14] and huNKG2D (see below) show the two monomers related by perfect, crystallographic dyad axes. However, the exact 2-fold symmetry of the NKG2D homodimer is broken in all three complex structures, with deviations of up to nearly 5° in directions both parallel and perpendicular to the homodimer dyad axis (Figure 4). These deviations accommodate the ridge, or peak, at the kink in the ligand α2-domain helix and allow the NKG2D homodimer to close over the ligand. However, these mo-

areas, and MIC-A residues in the disordered loop are represented by a checkerboard area. The conserved positions of the NKG2Dbinding site core residues are labeled in blue, and ligand-contacting residues in the receptors that vary in sequence between the human and murine proteins have tags highlighted with red borders. Sequence substitutions between ligand loci/alleles/isoforms are indicated by dashed arrows, with conservative substitutions labeled in green and nonconservative substitutions or deletions labeled in red.

Bottom: the complex interfaces are represented as above, except that the size of each residue label has been scaled by the energetic contribution the corresponding residue makes to the interaction; interactions with values less than 1.0 kcal/mol are not considered to constitute binding site hotspots and are not shown. NKG2D hotspots are predicted to lie within 7.4 to 1.1 kcal/mol when complexed with MIC-A; 4.6 to 1.3 kcal/mol when complexed with ULBP3; and 5.2 to 1.1 kcal/mol when complexed with RAE-1β. Ligand hotspots are predicted to lie within 5.0 to 1.0 kcal/mol for MIC-A; 5.2 to 1.0 kcal/mol for ULBP3; and 5.9 to 1.3 kcal/mol for RAE-1β.

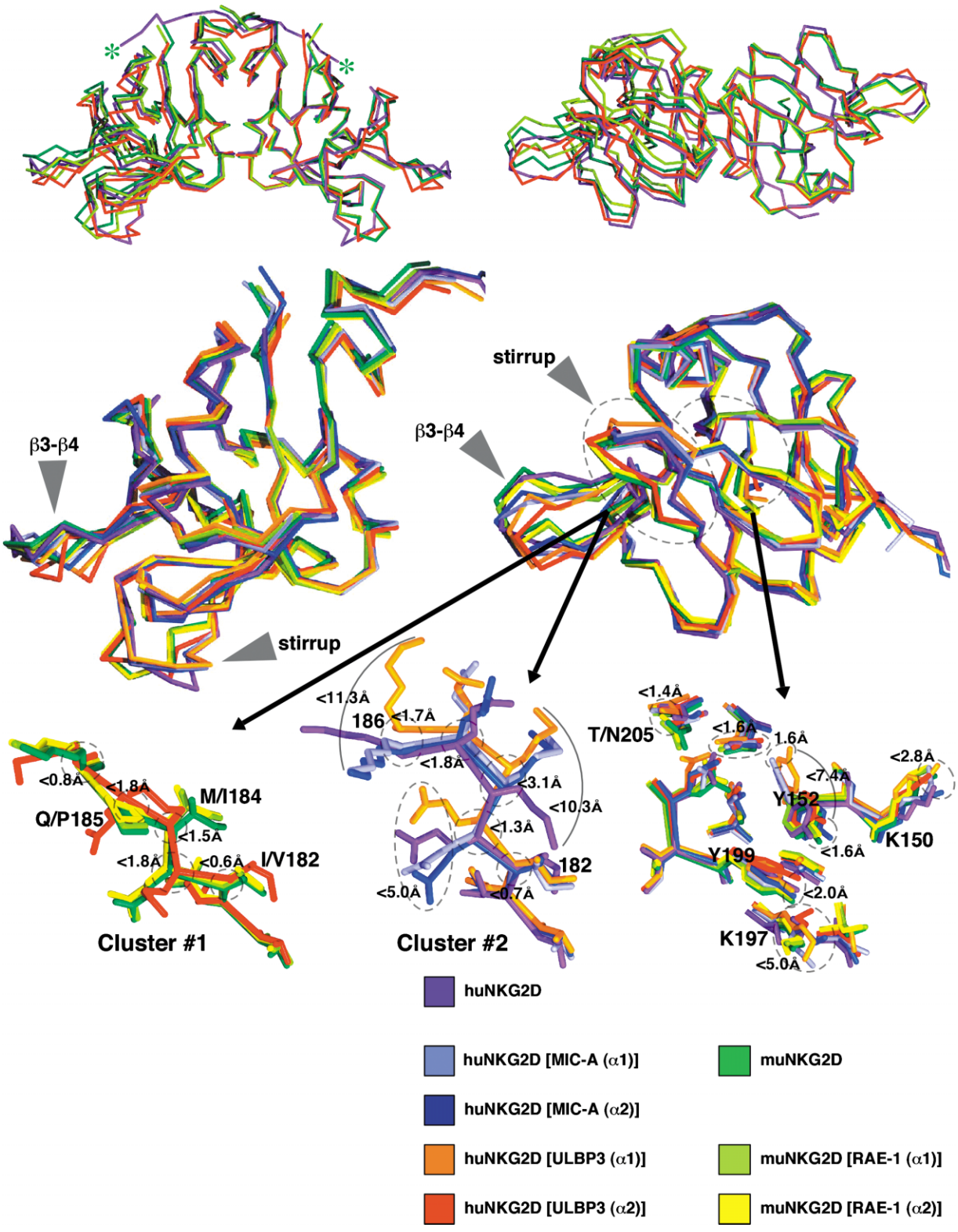

Figure 4. Structure of huNKG2D

Superpositions of the Cα backbones of the various structures of NKG2D, based on all common Cαs in a monomer, are shown, colored as indicated. At top, NKG2D homodimers are superimposed, in two orthogonal views left (asterisks indicate the N termini of free huNKG2D) and right, highlighting the variation in the homodimer interface angle. In the middle, all eight NKG2D monomer structures are superimposed, again in two orthogonal views left and right, highlighting the elements of flexibility in the protein. The β3-β4 and stirrup loops are indicated. At bottom, expanded views of the stirrup loop (left, cluster #1; center, cluster #2) and the side chains of ligand-contacted residues on the body of the NKG2D NKD (right) are shown. Distances illustrate the structural variance of the indicated atoms.

tions also do not contribute to an induced-fit mechanism in that they do not differentially alter the ligand-contacting surface on the receptor by inducing a more ligand-complementary shape on the NKG2D binding site, but rather simply position each NKG2D binding half-site over the appropriate cognate ligand surface.

Several loops in the structure show above average B factors and/or multiple conformations between structures, implying flexibility (Figure 4). Corresponding Cα atoms of the β3-β4 loop (residues 160–165 in huNKG2D, and 176–181 in muNKG2D) differ by 2 to 6 Å and have above average B factors, but this loop does not contact ligand. However, the β5-β5′ stirrup loop (residues 182–188 in huNKG2D, and 198–204 in muNKG2D) does make multiple contacts to the ligand in all six half-sites. The backbone of this loop essentially adopts one of two conformations among the eight NKG2D models (Figure 4): one cluster (#1) contains all the muNKG2D structures and the huNKG2D α2 monomer from the complex with ULBP3; the other cluster (#2) contains the remaining huNKG2D models. The cluster #1 conformation moves the loop outward, away from the center of mass of the complex, with Cα-to-Cα movements of almost 5 or 6 Å at residues 184 and 185, creating a wider binding saddle than the cluster #2 conformation. The differences in loop backbone structure do not stem from a hinged motion of the ends of the loop, but have differences distributed throughout the loop. A number of sequence differences between the human and murine receptors occur in loop residues (Ile182/Val198, Met184/Ile200, and Gln185/Pro201; huNKG2D/muNKG2D) and the largest differences between Cαs within or between the two clusters occur at some of these variable positions (almost 5 Å at 184/200 and over 6 Å at 185/201 across both clusters). These sequence differences likely affect loop conformation: Gln185 in the huNKG2D displays ϕ values ($-120°$ to $-155°$) outside of that allowed for prolines, as in muNKG2D; and β-branched Ile200 in all the muNKG2D models (and Met184 in huNKG2D-A from the ULBP3 complex), as in cluster #1, display β strand ϕ/ψ values, while Met184 in the rest of the huNKG2D models (cluster #2) displays generously allowed α-helical values. These differences in loop conformation were invoked to explain the observation that huNKG2D does not bind Rae-1β, whereas muNKG2D binds MIC, the result of a projected clash between huNKG2D residue Met184 and several Rae-1β residues in a hypothetical complex, due to the much more toed-in, or closed, huNKG2D stirrup loop conformation [13].

Relatively smaller structural variabilities are associated with the side chain conformations of some ligand-contacting residues (Figure 4). Cluster #2 stirrup loop residues Met184 and Lys186 have distal atom (Cε or Nζ) positions that differ by over 10 Å, with other residues' distal atoms differing by almost 5 Å. Side chain structural variation is generally more limited at the remaining cluster #2 positions and at the cluster #1 residues, and much more limited for ligand-contacting residues on the body of the NKD. For the latter residues, the largest variations are seen at the Nζ atoms of two lysines (150 and 197 in huNKG2D) and in alternate rotamer utilization by Tyr152, a binding site core residue. The remainder of the ligand-contacting residues have well-overlapping structures.

Table 1. Crystallographic Data Collection and Refinement Statistics

Space group	$P4_12_12$
Cell dimensions (Å)	a = b = 87.65, c = 36.13
Data Collection and Processing	
Wavelength	Cu Kα
Resolution (Å)	2.50 (2.59–2.50)
Unique reflections	5057 (466)
Redundancy	21.1
Completeness (%)	96.5 (90.1)
$<I/\sigma(I)>$	20.2 (6.8)
R_{sym}	0.066 (0.199)
Refinement	
Resolution (Å)	20–2.50 (2.59–2.50)
Reflections (all F > 0)	4838
Protein atoms	1030
Solvent atoms	104
Phosphate atoms	5
R_{cryst} (%)	24.5
R_{free} (%) (on 498 reflections)	29.6
Average B factor (Å^2)	39.4
Crossvalidated σ_A coordinate error (Å)	0.53
Rmsd from Ideal Geometry	
Bond length (Å)	0.008
Bond angles (°)	1.9
Dihedrals (°)	26.4
Impropers (°)	1.4
Ramachandran Statistics	
Most favored (%)	78.1
Additional allowed (%)	21.1
Generously allowed (%)	0.9
Disallowed (%)	0

Numbers in parentheses indicate values for the highest resolution shell.

As a specific example, the hydrogen bond partner atom of the human/murine substituted (threonine/asparagine) residue at position 205/221 (human/murine) falls within 1.4 Å across all the NKG2D structures (Figure 4).

The Structure of Free huNKG2D

Because the stirrup loop and certain side chains of the NKG2D binding site residues represent flexible elements that may contribute to a classical induced-fit interaction, we determined the crystal structure of unliganded huNKG2D at 2.5 Å resolution (Table 1) to analyze their ground-state conformations. Diffraction data were collected with Cu-Kα radiation from cryopreserved crystals of a soluble, recombinant form of huNKG2D encompassing nearly the entire ectodomain (residues 80–216), crystallized at a pH of 9, and phased by molecular replacement. The asymmetric unit contains half a homodimer.

The free huNKG2D monomer is, as expected, very similar to the other views of the NKG2D structure, with pairwise rms deviations between 1.1 and 1.4 Å on all common Cαs. Electron density is observed for more of the flexible N-terminal stalk than in any other structure, to Gln88. The stalk crosses over the homodimer interface, making fairly extensive contacts to the NKD of the other monomer in the homodimer and to neighboring monomers in the asymmetric unit, with the two homodimer-related stalk N termini spanning a distance of 49 Å, nearly the width of the whole molecule. In this most fully resolved view, the stalk displays no defined secondary

structure, and the only contacts between stalks of the same homodimer are van der Waals bonds involving residues 97–99 near the interface between monomers in the homodimer. The extreme flexibility of the N-terminal stalk, and the lack of any obvious, consistent associations between stalks or stalk and NKD, leaves us without an obvious structural mechanism for signaling ligand engagement to the interior of the cell.

In general, all other aspects of the structure of free huNKG2D, such as the β3-β4 loop and the ligand-contacting residues on the body of the NKD, fall within the variation already observed among the previous structures of NKG2D (Figure 4). The conformation of the free huNKG2D stirrup loop backbone clearly falls within cluster #2 (though the side chains of Met184 and Lys186 are somewhat divergent) and the side chain of Tyr152 adopts the more commonly observed rotamer. Slight differences between free and bound huNKG2D are observed at the homodimer interface, which is more open and packed more loosely in free huNKG2D, allowing for slight half-site movements (toeing-in) during complex formation. The only homodimer interface residue displaying a conformation outside of the range observed in the other NKG2D structures is Phe113, which was observed in two rotamers in the free huNKG2D structure: one similar to the other structures and the other pointing away from the ligand and packing into a different interface pocket (lined by residues Ile104 and Gln112 of the same monomer and Tyr106, Asp144, and Leu145 of the dimer-related monomer).

Computational Alanine-Scanning Mutagenesis

Because the NKG2D-ligand interfaces contain both structurally conserved and varying elements, recognizing highly structurally disparate ligands, we sought a systematic method for evaluating the relative contribution of each element. Binding energy is often distributed unevenly across protein-protein interfaces, with the largest changes in affinity occurring when so-called hotspot residues are mutated [28, 29]. Classically, alanine-scanning mutagenesis coupled to studies of binding energetics provides such information [30]. Here, we alternately conduct such an analysis in silico, using a method [31] validated by its use in engineering a novel protein-protein interface [32] and by selected evaluation of in vitro alanine mutations reported here. Briefly, computational alanine-scanning mutagenesis uses a simple physical model to score a series of receptor-ligand interfaces in which contact residues are individually replaced with alanine. After each alanine mutation, side chains at the interface are repacked with favorable rotamers and the resulting binding energy is calculated. The model was parameterized using results from 743 alanine mutagenesis experiments in monomeric proteins (data taken from the PROTHERM database [33]), and tested against a further 223 alanine-scanning mutations in 19 protein-protein complexes, with an average unsigned error of 1.09 kcal/mol [31].

Computational alanine-scanning analyses were conducted on the three NKG2D-ligand interfaces (Figure 2). A residue was defined as a binding hotspot if the resulting calculated difference in $\Delta\Delta G$ when mutated to alanine was at least 1 kcal/mol (the average value for all interface residues across the three complexes was 1.2 kcal/mol, with values ranging up to 7.4 kcal/mol at Tyr199 of the α1 huNKG2D monomer in the MIC-A complex). Nine to seventeen hotspots are scattered across each interface, with receptor and ligand hotspots generally correlated. Hotspot distribution is clearly asymmetric, indicating that one half-site dominates each interaction (the α1 site in the MIC-A complex, and the α2 site in the ULBP3 and Rae-1β complexes; Figure 2).

A dominant proportion of the binding energy on the receptor is invested in the two binding site core tyrosine residues at every NKG2D half-site, Tyr152/168 and Tyr199/215 (hu/muNKG2D). All but one of these central tyrosine residues in all six half-sites were classified as hotspots, with predicted changes in binding energy upon alanine mutation ranging from 1.5 to 7.4 kcal/mol. The third member of the common binding site core, the stirrup loop residue Met184/Ile200 (hu/muNKG2D), was not identified as a hotspot at any half-site. The second most commonly conserved receptor hotspot (four of the six half-sites) is Lys197/213 (hu/muNKG2D), which participates in a salt bridge in three of four cases. Only one NKG2D stirrup loop residue in one half-site, Gln185 in the α1 half-site of the MIC-A complex, is identified as a hotspot (2.2 kcal/mol). Conversely, on the ligand surfaces, two hotspots contact the stirrup loop ($>$2 kcal/mol; Arg74 in MIC-A and Arg82 in ULBP3), but these residues also interact, through salt bridges and/or H bonds, with non-stirrup loop residues.

Hotspots identified by the computational alanine-scanning analysis also correlate with ligand receptor-contacting residue conservation among alleles, loci, or isoforms (Figure 2). Of the 26 ligand residues that contact the NKG2D binding core residues (Tyr152/168, Met184/Ile200, and Tyr199/215), ten are conserved or only conservatively substituted, with an average energetic contribution of 2.1 kcal/mol. The other 16 core-contacting residues are nonconservatively substituted in at least one sequence, and are predicted to have a lower average contribution, 1.3 kcal/mol. Out of these, any residues that are deleted in any sequence on average contribute least, only 0.72 kcal/mol. The reason for the unusual polymorphism patterns in NKG2D ligands is unknown, but polymorphism is not predicted to significantly affect NKG2D binding: none of the MIC allelic substitutions at NKG2D contact positions have been experimentally shown to significantly affect affinity [34], and Rae-1 isoforms differ in NKG2D affinity only modestly, by about 2-fold [18]. Whereas MHC class I polymorphisms are closely coupled to function, directly determining peptide and TCR specificity, MIC polymorphisms have been difficult to reconcile with the interaction with NKG2D [15], and may reflect effects on currently uncharacterized interactions with other receptors, such as γδ TCRs [35].

Site-directed mutagenesis of MIC-A followed by surface plasmon resonance (SPR) biointeraction analysis provides additional validation of the computational alanine-scanning method (Table 2). MIC-A mutants, with residues at the binding interface (selected to span the range of interaction types and predicted strengths) individually mutated to alanine, were immobilized on SPR sensor chips. Measured huNKG2D equilibrium SPR re-

Table 2. Comparison of In Vitro and In Silico Free Energy Values

	K_d (μM)[a]	Std. Error[b]	Std. Deviation[c]	ΔG (kcal/mol)[d]	In Vitro $\Delta\Delta G$ (kcal/mol)	In Silico $\Delta\Delta G$ (kcal/mol)
MIC-A Mutation						
Wild-type	0.8	0.09	0.07	−8.3	—	—
K71A	1.8	0.2	0.9	−7.8	0.5	0.4
R74A	16.7	2.3	2.2	−6.5	1.8	5.0
M75A	6.3	1.2	0.8	−7.1	1.2	1.2
T155A	4.3	0.7	2.2	−7.3	1.0	2.0
H158A	0.4	0.06	0.21	−8.7	−0.4	0.1
ULBP3 Mutation[e]						
Wild-type	4			−7.4	—	—
H21A	30			−6.2	1.2	1.6
E76A	105			−5.4	1.9	1.0
R82M[f]	233			−5.0	2.4	2.0
D169A	77			−5.6	1.8	5.2

[a] Mean of two to four independent experiments.
[b] Mean of standard errors from two to four fits of response at equilibrium versus [NKG2D].
[c] Standard deviation of two to four independent experiments.
[d] $\Delta G = -RT \ln (K_d)$; $\Delta\Delta G = \Delta G_{mutant} - \Delta G_{wild\text{-}type}$
[e] K_d values as reported by Radaev et al. [21]. Standard errors were not reported. Temperature is assumed to be 25°C.
[f] This methionine mutation represents a significant reduction of affinity that can be compared to the predicted effect of an alanine mutation.

sponses at 25°C over these chips were used to derive ΔG and $\Delta\Delta G$ values. The experimentally determined values agree with the computational alanine-scanning technique to within 1 kcal/mol in four out of five cases (Table 2). Previously published SPR measurements of the affinities between huNKG2D and four ULBP3 mutants [21] provide further validation, with three of the four experimentally derived $\Delta\Delta G$ values matching the in silico values within 1 kcal/mol. In both studies, the largest deviations occurred at ligand positions involved in electrostatic interactions (R74A in MIC-A and D169A in ULBP3), perhaps reflecting the complexity of calculating electrostatic effects. However, the in silico method correctly predicted the presence or absence of hotspots at all nine mutation sites and correctly estimated the scale for seven of these.

Discussion

The ligand binding site on an NKG2D monomer is capable of extensive interactions with a broad array of structurally and sequence-divergent target surfaces on MHC class I-like cell surface proteins. These degenerate interactions must be specific enough to prevent inappropriate activation of effector functions. The simplest explanation invokes a classical induced-fit recognition mechanism to account for receptor degeneracy, and there are, indeed, multiple elements of flexibility in the receptor ligand binding site observed across the various crystal structures of NKG2D. These elements include a cluster of side chains on the body of the NKD of NKG2D that vary as to rotamer utilization and absolute conformation, and an apparently mobile loop.

However, the crystal structure of free huNKG2D, undertaken to determine the ground-state structure of these flexible elements, shows that the unliganded conformations of the side chains on the body of the NKD fall squarely within the range observed in the other structures of NKG2D, even for such potentially variable side chains as lysines. The variation is somewhat greater than the inherent coordinate accuracy of these crystal structures (estimated to range from 0.25 to 0.69 Å when reported), though not dramatically so in most cases. The one exception is the side chain of Tyr152/168, which adopts an alternate rotamer in two of eight structures. The stirrup loop, at least in terms of the backbone, also appears limited to only two fairly tightly clustered conformations. Therefore, the actual flexibility available to NKG2D immunoreceptors is somewhat limited.

In silico and in vitro analysis of the relative contributions that particular residue-residue contacts make to the overall interaction shows that, consistent with many protein-protein interfaces, the energy is unevenly distributed over the NKG2D-ligand interfaces, resulting in obvious binding hotspots and the domination of one half-site in each complex in the overall interaction. Binding hotspots are also overwhelmingly associated with structurally conserved elements of NKG2D and residues relatively conserved in the sequences of the ligand families. The most conserved hotspots across the NKG2D binding sites are the core binding residues Tyr152/168 and Tyr199/215, though these residues mediate different interactions among the ligands.

The conclusion drawn from these data is that NKG2D-mediated ligand recognition is not accomplished through what would be considered a classical induced-fit mechanism. NKG2D flexibility, when available, does not contribute to significant, hotspot level increases in binding. Consider Tyr152: when the alternate rotamer is selected (the α1 half-site of the MIC-A complex and the α2 half-site of the ULBP3 complex), the result is a reduction in the contribution to binding energy. Retention of the preferred rotamer would result in deleterious steric clashes in these two half-sites (with Met75 of MIC-A or Leu83 of ULBP3); therefore, this limited conformational flexibility is utilized to eliminate negative interactions rather than establish alternate strong, positive interactions. The "wiggle" displayed by the side chains on the body of the NKD is likely to contribute to binding (and the high Sc values) by optimizing van der Waals interac-

tions at the interface, but the movements are small compared to those typically seen for induced-fit binding, which are also generally concurrent with significant backbone rearrangements.

The stirrup loop is an obvious candidate element when considering induced-fit binding, and clearly increases the surface area buried (and therefore extends both the van der Waals interaction network and the displacement of ordered waters) at the interfaces, but the computational analysis shows that only one residue in all six half-site structures constitutes even a minor binding hotspot. However, the stirrup loop may not, in actuality, represent a significantly flexible element. Stirrup loop backbone conformations cluster in two groupings that, with one exception (the α2 ULBP3 half-site), are divided between huNKG2D and muNKG2D, with human/murine loop sequence differences directly affecting backbone conformation. If the huNKG2D stirrup is flexible, capable of adopting both cluster #1- and cluster #2-like conformations, as suggested by the exceptional α2 ULBP3 half-site structure, then the observation that huNKG2D does not bind the murine ligand Rae-1β is difficult to understand; huNKG2D should then be able to adopt a toed-out conformation compatible with Rae-1β binding.

This apparent contradiction can be resolved if the exceptional conformation of the human stirrup loop in the ULBP3 complex reflects model bias inadvertently introduced during the crystallographic analysis rather than a real alternate conformation. If this is so, then the stirrup loop may not have a flexible backbone at all, merely two different conformations in huNKG2D and muNKG2D, with particular conformations potentially affecting ligand selection. In support of this supposition, we note that this structure was phased, in part, by molecular replacement with the free muNKG2D structure and that this loop displays the highest B factors in the huNKG2D-ULBP3 complex structure: the average B factor for the aberrant stirrup loop, even while stabilized by extensive contacts with ligand, is 85 Å^2 versus 39 Å^2 for the structure as a whole or 31.0 Å^2 for the homodimer-related stirrup loop; in contrast, in free huNKG2D, the stirrup loop has an average B factor of 42.7 Å^2 versus 39.4 Å^2 overall, even while making fairly limited crystal contacts. Contradicting this supposition is the clear evidence that model bias did not affect the modeling of the dimer-related stirrup loop in the ULBP3 complex, and that the relevant statistics show that the model has been well-refined overall.

Another possibility is raised by the free MIC-A structure, in which a portion of the NKG2D binding site, a stretch of the α2 domain helix (residues 152–161), is disordered [11]. This section is ordered in the complex structure (Figure 2). Three minor ligand hotspots are located either in the middle of this sequence (Thr155) or flanking it (Asp149 and Asp163). This transition from disorder to apparently a single ordered state suggests that flexibility in the MIC-A *ligand* is accommodating the *receptor*. However, the corresponding parts of MIC-B and Rae-1β are clearly more ordered in the unliganded state. Besides this, such flexibility in a ligand would only allow it to accommodate a range of receptors, not the reverse. Thus, this phenomenon is unique to MIC-A and cannot contribute to NKG2D degeneracy.

To recapitulate, our analysis indicates that the energetically dominant interactions in NKG2D-ligand interfaces are formed by a structurally conserved consensus binding site on the receptor that interacts in different ways with its various protein ligands. We further suggest that the symmetry of the NKG2D homodimer is broken energetically when recognizing its asymmetric ligands, with one of the NKG2D subunits contributing the majority of the binding free energy. The phenomenon that ligands can utilize different strategies to bind to a structurally conserved binding site is reminiscent of the common site of Fc fragment of human IgG interacting with four structurally extremely diverse protein partners [17], and has also been seen for different small molecules binding to the same protein site [36–38]. Thus, NKG2D-mediated interactions appear to follow a general principle of protein interactions different from the classical concept of induced fit.

Biological Implications

The C-type lectin-like immunoreceptor NKG2D mediates crucial antitumor and antiviral responses by NK cells and $\alpha\beta$ and $\gamma\delta$ T cells by recognizing a diverse set of MHC class I-like ligands with affinities that are notably stronger than other immunoreceptor-ligand interactions. NKG2D homodimers recognize their asymmetric, monomeric ligands with a single, equivalent, overlapping binding site on each receptor monomer to interact with distinct, nonconserved ligand surfaces, yielding 2:1 complexes. This raises a profound conundrum: how does this single binding site achieve such degeneracy while retaining the immunologically required specificity and relatively tight affinity? Whereas NKG2D appears to display multiple degrees of flexibility in its ligand-contacting elements, consistent with a classical induced-fit recognition mechanism, close inspection of the available crystal structures suggests that many degrees of flexibility in the molecule are irrelevant for ligand binding or may be more constrained than originally thought. The crystal structure of unliganded human NKG2D defines the ground-state conformation for ligand-contacting flexible elements, confirming that many of the apparently ligand-induced structural rearrangements are more subtle than seen in other cases of induced-fit binding. Ranking the relative contribution each individual interaction makes to binding by in silico and in vitro alanine-scanning mutagenesis analyses shows that binding hotspots are asymmetrically arranged across NKG2D homodimers and most often associated with structurally conserved elements and residues conserved within NKG2D ligand sequence families. Minor rearrangements of ligand-contacting side chains therefore appear to either simply optimize the binding interfaces or eliminate potentially serious steric clashes, but are not associated with significant energetic contributions to binding. Distinct from a classical induced-fit mechanism on the receptor site, our analysis suggests that the divergent ligands have evolved different strategies for complementary binding to a relatively small consensus hotspot site on NKG2D, as could be general for many protein-protein interfaces.

Experimental Procedures

Protein Expression, Purification, and Crystallization

The extracellular domains of human NKG2D (residues 80–216) and MIC-A (residues 1–276) were expressed in BL21-DE3 or BL21-DE3-RIL bacteria (Stratagene), respectively, as inclusion bodies, denatured, refolded, and purified as previously described [16]. MIC-A mutations were introduced with the QuickChange site-directed mutagenesis kit (Stratagene) following the manufacturer's protocol. Free huNKG2D crystals were grown serendipitously in attempts to cocrystallize huNKG2D-ULBP1 complexes. Protein solutions containing 5 mg/ml huNKG2D and 4 mg/ml ULBP1 (mixed in a 2:1 molar ratio) in 25 mM PIPES (pH 7.0), 150 mM NaCl, 1 mM EDTA, and 0.02% NaN_3 were equilibrated by vapor diffusion at 291K in a sitting drop geometry over wells containing 1.6 M ammonium dihydrogen phosphate and 10% ethylene glycol buffered with 100 mM bicine (pH 9.0). Crystals grew overnight.

Crystallography

Crystals were transferred to a solution of the mother liquor plus 15% ethylene glycol as a cryoprotectant and flash-cooled in a nitrogen gas stream at 100K. Diffraction data were collected on a Rigaku R-AXIS IV area detector, processed with DENZO, and scaled with SCALEPACK from the HKL suite [39]. Initial phases were generated by molecular replacement using EPMR [40] with one NKG2D monomer from the huNKG2D-MIC-A complex crystal structure (Protein Data Bank, PDB [41]; accession code 1HYR), with residues 161–164 and 183–187 removed, as the search model. The structure was rebuilt with the xfit module from the XtalView software suite [42] using composite omit maps calculated with the crystallography and NMR system (CNS) [43]. Simulated-annealing torsional refinement using the maximum likelihood target function mlf was carried out in CNS, followed by alternate rounds of rebuilding, positional, and group B factor refinement. Individual B factor and bulk solvent corrections were applied in the later stages of refinement. Refinement progress was monitored using R_{cryst} and R_{free} [44]. Data collection and refinement statistics are shown in Table 1.

Computational Alanine Scanning

Binding free energy changes upon alanine mutation ($\Delta\Delta G_{bind}$) are calculated using the equation

$$\Delta\Delta G_{bind} = \Delta G^{MUT}_{bind} - \Delta G^{WT}_{bind} \quad (1)$$

$$= (\Delta G^{MUT}_{complex} - \Delta G^{MUT}_{partnerA} - \Delta G^{MUT}_{partnerB}) - (\Delta G^{WT}_{complex} - \Delta G^{WT}_{partnerA} - \Delta G^{WT}_{partnerB}) \quad (2)$$

where $\Delta G_{complex}$, $\Delta G_{partner\,A}$, and $\Delta G_{partner\,B}$ are the stabilities of the complex and the unbound partners, and WT and MUT denote wild-type and mutant proteins. Protein stabilities (ΔG) are calculated using an all-atom representation of the protein (including all heavy atoms as well as polar hydrogens) and a free energy function dominated by van der Waals packing interactions, an implicit solvation potential, and hydrogen bonding [31].

Side chain conformational changes upon complex formation and mutation were modeled using side chains represented as rotamers from a backbone-dependent library [45] on a fixed backbone template, as described previously [31]. In brief, different rotamer conformations (including the X-ray coordinates of the native side chains at each position) were allowed for all residues with at least one side chain atom within a sphere of 5 Å radius of the site of mutation. The conformations of all other amino acid side chains were taken unchanged from the parent crystal structures. Global optimization of side chain conformations was performed using the energy function given in Equation 2 and a Monte Carlo-simulated annealing procedure [46], in which a move consisted of the replacement of a randomly picked side chain rotamer at a single position by another rotamer from the library.

SPR Interaction Analysis

SPR measurements were done with a Biacore 3000 biosensor (Biacore AB) in standard HBS-EP buffer. To insure monodispersivity, proteins were subjected to an additional size exclusion chromatography step, in 10 mM HEPES (pH 7.4), 150 mM NaCl, and 3 mM EDTA (HBS-E), within 48 hr of analysis. Protein concentrations were measured by BCA assay (Pierce) and 0.005% surfactant P20 was added. Proteins were coupled to CM5 research grade gold biosensor chips using amine coupling chemistry; HLA-G was coupled as a concurrent negative control. huNKG2D was injected at 30 μL/min in six to nine concentrations ranging from 125 to 0.125 μM at 25°C. Ligand dissociation was fast and complete enough that explicit regeneration was unnecessary. K_ds were calculated from the best-fit line to a plot of average response at equilibrium versus NKG2D concentration using BIAevaluation 3.0 software.

Acknowledgments

B.J.M. is a Cancer Research Institute postdoctoral fellow; T.K. is a postdoctoral fellow of the Human Frontiers Science Program and the European Molecular Biology Organization. This work was supported by NIH grant AI48675 (R.K.S.). The authors would like to thank Christopher O'Callaghan for a critical review of the manuscript.

Received: October 3, 2002
Revised: January 7, 2003
Accepted: February 5, 2003
Published: April 1, 2003

References

1. Moretta, L., Bottino, C., Pende, D., Mingari, M.C., Biassoni, R., and Moretta, A. (2002). Human natural killer cells: their origin, receptors and function. Eur. J. Immunol. *32*, 1205–1211.
2. Kogelberg, H., and Feizi, T. (2001). New structural insights into lectin-type proteins of the immune system. Curr. Opin. Struct. Biol. *11*, 635–643.
3. Natarajan, K., Dimasi, N., Wang, J., Mariuzza, R.A., and Margulies, D.H. (2002). Structure and function of natural killer cell receptors: multiple molecular solutions to self, nonself discrimination. Annu. Rev. Immunol. *20*, 853–885.
4. Lanier, L.L. (2000). Turning on natural killer cells. J. Exp. Med. *191*, 1259–1262.
5. Raulet, D.H., Vance, R.E., and McMahon, C.W. (2001). Regulation of the natural killer cell receptor repertoire. Annu. Rev. Immunol. *19*, 291–330.
6. Cerwenka, A., and Lanier, L.L. (2001). Natural killer cells, viruses and cancer. Nat. Rev. Immunol. *1*, 41–49.
7. Leong, C.C., Chapman, T.L., Bjorkman, P.J., Formankova, D., Mocarski, E.S., Phillips, J.H., and Lanier, L.L. (1998). Modulation of natural killer cell cytotoxicity in human cytomegalovirus infection: the role of endogenous class I major histocompatibility complex and a viral class I homolog. J. Exp. Med. *187*, 1681–1687.
8. Moretta, A., Bottino, C., Vitale, M., Pende, D., Cantoni, C., Mingari, M.C., Biassoni, R., and Moretta, L. (2001). Activating receptors and coreceptors involved in human natural killer cell-mediated cytolysis. Annu. Rev. Immunol. *19*, 197–223.
9. Pardoll, D.M. (2001). Immunology. Stress, NK receptors, and immune surveillance. Science *294*, 534–536.
10. Strong, R.K. (2002). Asymmetric ligand recognition by the activating natural killer cell receptor NKG2D, a symmetric homodimer. Mol. Immunol. *38*, 1029–1037.
11. Li, P., Willie, S.T., Bauer, S., Morris, D.L., Spies, T., and Strong, R.K. (1999). Crystal structure of the MHC class I homolog MIC-A, a γδ T cell ligand. Immunity *10*, 577–584.
12. Radaev, S., Rostro, B., Brooks, A.G., Colonna, M., and Sun, P.D. (2001). Conformational plasticity revealed by the cocrystal structure of NKG2D and its class I MHC-like ligand ULBP3. Immunity *15*, 1039–1049.
13. Li, P., McDermott, G., and Strong, R.K. (2002). Crystal structures of RAE-1β and its complex with the activating immunoreceptor NKG2D. Immunity *16*, 77–86.
14. Wolan, D.W., Teyton, L., Rudolph, M.G., Villmow, B., Bauer, S., Busch, D.H., and Wilson, I.A. (2001). Crystal structure of the

murine NK cell-activating receptor NKG2D at 1.95 Å. Nat. Immunol. *2*, 248–254.
15. Holmes, M.A., Li, P., Petersdorf, E.W., and Strong, R.K. (2002). Structural studies of allelic diversity of the MHC class I homolog MIC-B, a stress-inducible ligand for the activating immunoreceptor NKG2D. J. Immunol. *169*, 1395–1400.
16. Li, P., Morris, D.L., Willcox, B.E., Steinle, A., Spies, T., and Strong, R.K. (2001). Complex structure of the activating immunoreceptor NKG2D and its MHC class I-like ligand MICA. Nat. Immunol. *2*, 443–451.
17. DeLano, W.L., Ultsch, M.H., de Vos, A.M., and Wells, J.A. (2000). Convergent solutions to binding at a protein-protein interface. Science *287*, 1279–1283.
18. O'Callaghan, C.A., Cerwenka, A., Willcox, B.E., Lanier, L.L., and Bjorkman, P.J. (2001). Molecular competition for NKG2D: H60 and RAE1 compete unequally for NKG2D with dominance of H60. Immunity *15*, 201–211.
19. Boyington, J.C., Motyka, S.A., Schuck, P., Brooks, A.G., and Sun, P.D. (2000). Crystal structure of an NK cell immunoglobulin-like receptor in complex with its class I MHC ligand. Nature *405*, 537–543.
20. Fan, Q.R., Long, E.O., and Wiley, D.C. (2001). Crystal structure of the human natural killer cell inhibitory receptor KIR2DL1-HLA-Cw4 complex. Nat. Immunol. *2*, 452–460.
21. Radaev, S., Kattah, M., Zou, Z., Colonna, M., and Sun, P.D. (2002). Making sense of the diverse ligand recognition by NKG2D. J. Immunol. *169*, 6279–6285.
22. Koshland, D.E., Jr. (1958). Mechanism of transfer enzymes. In The Enzymes, P. Boyer, et al., eds., Revised Edition (New York: Academic Press), pp. 305–315.
23. Rini, J.M., Schulze-Gahmen, U., and Wilson, I.A. (1992). Structural evidence for induced fit as a mechanism for antibody-antigen recognition. Science *255*, 959–965.
24. Garcia, K.C., Degano, M., Pease, L.R., Huang, M., Peterson, P.A., Teyton, L., and Wilson, I.A. (1998). Structural basis of plasticity in T cell receptor recognition of a self peptide-MHC antigen. Science *279*, 1166–1172.
25. Boniface, J.J., Reich, Z., Lyons, D.S., and Davis, M.M. (1999). Thermodynamics of T cell receptor binding to peptide-MHC: evidence for a general mechanism of molecular scanning. Proc. Natl. Acad. Sci. USA *96*, 11446–11451.
26. Reiser, J.B., Gregoire, C., Darnault, C., Mosser, T., Guimezanes, A., Schmitt-Verhulst, A.M., Fontecilla-Camps, J.C., Mazza, G., Malissen, B., and Housset, D. (2002). A T cell receptor CDR3β loop undergoes conformational changes of unprecedented magnitude upon binding to a peptide/MHC class I complex. Immunity *16*, 345–354.
27. Wu, L.C., Tuot, D.S., Lyons, D.S., Garcia, K.C., and Davis, M.M. (2002). Two-step binding mechanism for T-cell receptor recognition of peptide MHC. Nature *418*, 552–556.
28. Clackson, T., and Wells, J.A. (1995). A hot spot of binding energy in a hormone-receptor interface. Science *267*, 383–386.
29. Bogan, A.A., and Thorn, K.S. (1998). Anatomy of hot spots in protein interfaces. J. Mol. Biol. *280*, 1–9.
30. Manning, T.C., Schlueter, C.J., Brodnicki, T.C., Parke, E.A., Speir, J.A., Garcia, K.C., Teyton, L., Wilson, I.A., and Kranz, D.M. (1998). Alanine scanning mutagenesis of an $\alpha\beta$ T cell receptor: mapping the energy of antigen recognition. Immunity *8*, 413–425.
31. Kortemme, T., and Baker, D. (2002). A simple physical model for binding energy hotspots in protein-protein complexes. Proc. Natl. Acad. Sci. USA *99*, 14116–14121.
32. Chevalier, B.S., Kortemme, T., Chadsey, M.S., Baker, D., Monnat, R.J., Jr., and Stoddard, B.L. (2002). Design, activity and structure of E-DreI, a highly site-specific artificial endonuclease. Mol. Cell *10*, 895–905.
33. Gromiha, M.M., Uedaira, H., An, J., Selvaraj, S., Prabakaran, P., and Sarai, A. (2002). ProTherm, thermodynamic database for proteins and mutants: developments in version 3.0. Nucleic Acids Res. *30*, 301–302.
34. Steinle, A., Li, P., Morris, D.L., Groh, V., Lanier, L.L., Strong, R.K., and Spies, T. (2001). Interactions of human NKG2D with its ligands MICA, MICB, and homologs of the mouse RAE-1 protein family. Immunogenetics *53*, 279–287.
35. Wu, J., Groh, V., and Spies, T. (2002). T cell antigen receptor engagement and specificity in the recognition of stress-inducible MHC class I-related chains by human epithelial $\gamma\delta$ T cells. J. Immunol. *169*, 1236–1240.
36. Dennis, S., Kortvelyesi, T., and Vajda, S. (2002). Computational mapping identifies the binding sites of organic solvents on proteins. Proc. Natl. Acad. Sci. USA *99*, 4290–4295.
37. Mattos, C., and Ringe, D. (1996). Locating and characterizing binding sites on proteins. Nat. Biotechnol. *14*, 595–599.
38. Liepinsh, E., and Otting, G. (1997). Organic solvents identify specific ligand binding sites on protein surfaces. Nat. Biotechnol. *15*, 264–268.
39. Otwinowski, Z., and Minor, W. (1996). Processing of X-ray diffraction data collected in oscillation mode. Methods Enzymol. *276*, 307–326.
40. Kissinger, C.R., Gehlhaar, D.K., and Fogel, D.B. (1999). Rapid automated molecular replacement by evolutionary search. Acta Crystallogr. *D55*, 484–491.
41. Berman, H.M., Westbrook, J., Feng, Z., Gilliland, G., Bhat, T.N., Weissig, H., Shindyalov, I.N., and Bourne, P.E. (2000). The Protein Data Bank. Nucleic Acids Res. *28*, 235–242.
42. McRee, D.E. (1999). XtalView/Xfit—a versatile program for manipulating atomic coordinates and electron density. J. Struct. Biol. *125*, 156–165.
43. Brunger, A.T., Adams, P.D., Clore, G.M., DeLano, W.L., Gros, P., Grosse-Kunstleve, R.W., Jiang, J.S., Kuszewski, J., Nilges, M., Pannu, N.S., et al. (1998). Crystallography & NMR system: a new software suite for macromolecular structure determination. Acta Crystallogr. *D54*, 905–921.
44. Brunger, A.T. (1992). Free R value: a novel statistical quantity for assessing the accuracy of crystal structures. Nature *355*, 472–474.
45. Dunbrack, R.L., Jr., and Cohen, F.E. (1997). Bayesian statistical analysis of protein side-chain rotamer preferences. Protein Sci. *6*, 1661–1681.
46. Kuhlman, B., and Baker, D. (2000). Native protein sequences are close to optimal for their structures. Proc. Natl. Acad. Sci. USA *97*, 10383–10388.
47. Guex, N., and Peitsch, M.C. (1997). SWISS-MODEL and the Swiss-PdbViewer: an environment for comparative protein modeling. Electrophoresis *18*, 2714–2723.

Accession Numbers

The coordinates have been deposited in the Protein Data Bank under ID code 1MPU.